Int. J. Heat Mass Transfer. Vol. 32, No. 1, pp. 35–46, 1989
Printed in Great Britain

0017–9310/89 $3.00 + 0.00

Fluid flow and heat transfer in plasma reactors—II. A critical comparison of experimentally measured and theoretically predicted temperature profiles in plasma jets in the absence and presence of side-stream injection

A. H. DILAWARI,†§ J. SZEKELY,† J. F. COUDERT‡ and P. FAUCHAIS‡

† Department of Materials Science and Engineering, Massachusetts Institute of Technology, Cambridge, MA 02139, U.S.A.

‡ University of Limoges, 123 avenue Albert Thomas, 87060 Limoges Cedex, France

(*Received* 23 *September* 1987 *and in final form* 16 *May* 1988)

Abstract—A critical comparison is presented between experimental measurements and theoretical predictions describing the temperature profiles in a nitrogen plasma jet discharging into nitrogen, with a sideways-injected cold gas stream of nitrogen or oxygen. In general, the theoretical predictions, based on the solution of the axi-symmetric Navier–Stokes equations and associated thermal and mass balance relationships are found to be in good agreement with the measurements. A notable feature of the modelling work is that particular care had been taken to specify the temperature and the velocity profiles at the inlet boundary, chosen to be some distance inside the torch, and the thermal boundary conditions at the other bounding surfaces.

INTRODUCTION

IN A PREVIOUS paper [1], two of the present authors described a mathematical representation of heat and fluid flow phenomena and mixing in a confined plasma system, both in the presence and the absence of swirl; furthermore, the effect of side-stream injection has also been explored. In this previous paper, attention was focused on the computation, and no explicit comparison was made with the experimental measurements. The purpose of the present paper is to critically examine the comparison of the theoretical predictions of a closely related plasma system with experimental measurements, concerning the temperature fields within the system.

Such a critical comparison is clearly desirable, because the inherent complexity of plasma systems requires that a number of assumptions be made in the statement of the governing equations, as discussed earlier, and the appropriateness of these can only be assessed in the light of experimental data. Another important point that should be made here is that many 'real life' industrially used plasma systems involve annular or side-stream injection of various gaseous species, and it is necessary that the models to be used represent these systems also.

Over the last several years, increasing attention has been devoted to the mathematical modelling of the flow, temperature and turbulence fields in plasma jets issuing from the torch. The earlier work used the boundary-layer (parabolic) approach to represent the plasma free plume [2–5], which could not fully address the important feature of developing flow in the torch nozzle, flow in reactors or plasma flames impinging on targets. In refs. [3–6], an important phenomenon of the mixing of an exiting plasma jet with the ambient environment was either neglected, or only partially represented. Reference [7] successfully addressed this issue.

The temperature measurements are made in the free plume, with and without injection of cold gas in the torch nozzle. This ideally requires that the integration domain be extended for the full length of the arc column. However, as the point of injection of the cold gas is downstream from the point of attachment of the arc, the calculation domain inside the torch is extended only to the point where the influence of the flow of current is absent. (This condition has already been relaxed, and progress in this respect will be presented in a subsequent publication.)

STATEMENT OF THE PROBLEM

Figure 1 shows a schematic sketch of the system to be considered. This is seen to consist of a non-transferred arc plasma emerging from a nozzle into a very large cylindrical chamber. The ratio of the flow area of the chamber to that of the flow area of the torch orifice is large enough to consider the plasma

§ Visiting Fulbright Scholar, on leave of absence from Institute of Chemical Engineering and Technology, University of the Punjab, Lahore 20, Pakistan.

NOMENCLATURE

C_1, C_2, C_D constants in K–ε turbulence model
C_p specific heat
h enthalpy
H_1 torch nozzle length included in integration domain
H_2 free plume length included in integration domain
H_3 free plume width included in integration domain
k thermal conductivity
K turbulence kinetic energy per unit mass
m mass concentration of plasma gas (nitrogen)
P_w torch power
Q_i cold gas injection rate
Q_p plasma gas flow rate
r radial coordinate
R_0 internal radius of torch exit
S_ϕ source term for dependent variable
S_R radiation loss per unit volume of plasma
T_a ambient temperature
T_l left chamber wall temperature
T_m maximum temperature
T_t torch tip temperature
u_m velocity of plasma at $r = 0$ and $z = 0$ (maximum velocity)
v velocity in r-direction
z axial coordinate.

Greek symbols
ε dissipation rate of turbulence energy
η thermal efficiency of plasma torch
μ_l, μ_e, μ_t molecular, effective and turbulent viscosities, respectively
ρ density
σ turbulent Prandtl/Schmidt number for h, K, ε and m, respectively.

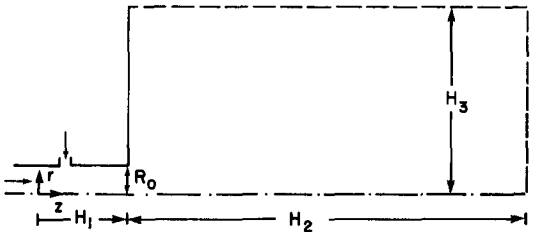

FIG. 1. Schematic sketch of the system.

jet as emerging from a nozzle into an infinite ambient environment. Such an assumption may not be truly valid if the system is made to run for an extended period for experimental measurements. In such a case, some uncertainties in specifying both the temperature and the concentration conditions at the entrainment boundary would exist. It may, however, be mentioned that the temperature of the chamber has been noted to be essentially the same as the ambient temperature, thereby suggesting that the radiated energy of the plasma is essentially absorbed by the water-cooled walls. The chamber is first pumped down to 1 Torr and then filled with the plasma gas to 1 atm pressure before the plasma is started.

In the experimental setup, different volumes of cold gas (nitrogen or oxygen) are injected into the torch through eight equally spaced radial holes (1 mm diameter) normal to the nozzle axis, and are located 5 mm upstream in the exit of the torch. This injection arrangement is approximated in the theoretical calculations by calculating the velocity of the injection gas on the basis of flow rate and total flow area of these eight holes, and then, using this velocity, calculating the width of the cylindrical port. This approximation is not likely to introduce any serious error, as the magnitude of the injection velocity is the main parameter expected to play a significant role, which is kept the same.

The flow inside the torch nozzle was considered laminar, as the Reynolds number, based on the maximum velocity, viscosity and density of the plasma at the maximum temperature, is lower than the critical value for flow to be turbulent. It is realized that this may be somewhat of an oversimplification since the very steep temperature gradients could well introduce flow instabilities; however, such instability may not give rise to fully turbulent flow. Furthermore, experimental measurements at the torch exit, and visual observations, suggested that the flow was laminar when exiting the torch. Because of the rapid quenching/decay of the jet, the flow in the free plume is expected to be turbulent, as has been experimentally observed. Therefore, the flow in the free plume is assumed turbulent, and an isotropic eddy viscosity in the stress–strain relationship holds. It should be remarked here that while the flow may be fully turbulent some short distance from the torch exit, it is expected to be transitional in the near vicinity of the torch exit. It follows that some error could be introduced using a high Reynolds number turbulence model [8].

A number of modifications of the standard K–ε turbulence model have been proposed to predict near-wall and low Reynolds number turbulent boundary layer flows [9–14]. However, before using such an approach, one requires at least a detailed map of velocity and turbulent quantities to critically determine the suitability of an adopted approach. Work is presently in progress both for experimental measurements of needed flow quantities, and for suitable modifications of the computer code.

The assumptions made that the plasma is in local thermodynamic equilibrium throughout, and is optically thin, and that compressibility effects are negligible, are not likely to involve significant error.

The case under study is a variable density–turbulent flow system. For such a system, two types of decomposition can be used: either the unweighted form commonly used for constant-density flows, or the density-weighted decomposition suggested by Favre [15]. In the present work, unweighted averaging is adopted, and as a first approximation the correlations involving density fluctuation are neglected. These correlations are not expected to introduce serious errors, as the level of turbulence is not large especially close to the nozzle exit, where the temperature decay may be maximum.

The plasma gas in the present study is always nitrogen, and nitrogen or oxygen is injected as a side stream. Thus, nitrogen plasma or a mixture of nitrogen and oxygen plasma exits the torch into nitrogen. Therefore, in the formulation of the mass transport equation, a binary system of nitrogen and oxygen is considered.

Following the aforesaid assumptions, the equations of conservation of mass, momentum, enthalpy h, plasma mass fraction m, turbulent kinetic energy K and turbulent energy dissipation rate ε, which govern the plasma flow under consideration, can be written in a general form, as these transport equations are all similar, as follows:

$$\frac{1}{r}\left\{\frac{\partial}{\partial z}(\rho ru\phi) + \frac{\partial}{\partial r}(\rho rv\phi) - \frac{\partial}{\partial z}\left(r\Gamma_\phi \frac{\partial \phi}{\partial z}\right) - \frac{\partial}{\partial r}\left(r\Gamma_\phi \frac{\partial \phi}{\partial r}\right)\right\} = S_\phi \quad (1)$$

where ϕ represents the two velocity components (r and z), as well as the other variables already mentioned; if ϕ is put equal to unity, and Γ_ϕ and S_ϕ to zero, this equation also represents the continuity equation. Forms for the source terms and transport coefficients for each of the variables are given in Table 1. Properties of the gases involved were taken from tabulated data of Fauchais [16] and Yos [17].

The turbulence model constants C_1, C_2, C_D, σ_K, σ_ε, σ_h and σ_m are given values recommended by Pun and Spalding [18] and are tabulated in Table 2.

The above equations alone do not specify the problem; additional appropriate information regarding boundary conditions is required.

BOUNDARY CONDITIONS

The transport equations of the form shown in equation (1) are elliptic, and thus require the statement of conditions on all boundaries of the solution domain shown in Fig. 1. At the inlet boundary, the plasma is assumed to have parabolic profiles for both axial velocity and temperature. The maximum values of axial velocity and temperature at the axis are selected to satisfy both mass and the energy input used in the experiment. The radial component of velocity is taken to be equal to zero. The plasma torch of this study is relatively short (i.e. $L/D = 5.3$), and the Reynolds number of flow gradually changes as the heat content of the flowing plasma changes due to Joule heating, convective and radiative heat loss; therefore, the flow develops both hydrodynamically and thermally throughout the length of the torch, suggesting the use of elliptic equations as adopted in the present work.

At the torch tip and left-solid boundary, the precise definition of the boundary conditions for all the dependent variables would necessitate solution of their respective equations through the semi-laminar region immediately adjacent to these solid boundaries. This would be expensive even if a low Reynolds number version of the model was available. One may avoid the need for detailed calculations in these near-solid boundary regions by introducing equations to link u, v, h, K and ε on the solid boundary to those in the logarithmic region. The normal velocity is set at zero, while the law of the wall is used for the parallel velocity to the solid boundary. This one-dimensional Couette flow, characteristic of the flow, is extremely useful. It also provides a way around these regions of steep nonlinear variation of the variable, and the fact that laminar and turbulent effects become of the same order of magnitude. These equations, called 'wall functions', are used in finite difference calculations at points near these solid boundaries. They occur in the momentum equations and K-generation terms with the appropriate near-wall ε specification. The solid-wall boundary condition formula for h suggested by Pun and Spalding [18] is used. As for the mass fraction of plasma, a mass flux equal to zero at the solid boundary is employed.

For the sideways stream, u is assigned a value of zero, while constant values for v and h are used, which take into account both the mass flow and energy of the injected cold gas. The value of m is fixed as 1 or 0, depending upon the nitrogen or oxygen gas being injected.

Along the entrainment boundary, which is placed sufficiently far away from the axis of symmetry, the static pressure is assumed constant (conveniently zero). The axial velocity is assumed zero, while the turbulent kinetic energy and its dissipation rate are assigned arbitrarily low values yielding an eddy viscosity $\mu_t = 5\mu_l$. It should be remarked here that for unconfined systems, the setting of the proper boundary conditions at the 'far surface' can be very important, because these will ultimately markedly influence the nature of the interaction (including entrainment) of the plasma jet with its environment. A good discussion by Leschziner and Rodi of these issues is available [19, 20]. The actual choice of the boundary conditions for k and ε was made after an extensive parametric study which suggested that their role was not very important, provided small enough values were chosen for them at these bounding surfaces.

Table 1. The transport coefficients and source terms

ϕ	Γ_ϕ	S_ϕ
1	0	0
u	$\mu_e = \mu_l + \mu_t$	$-\frac{\partial P}{\partial z} + \frac{1}{r}\frac{\partial}{\partial r}\left(r\mu_e \frac{\partial v}{\partial z}\right) + \frac{\partial}{\partial z}\left(\mu_e \frac{\partial u}{\partial z}\right)$
v	μ_e	$-\frac{\partial P}{\partial r} - \frac{2\mu_e v}{r^2} + \frac{1}{r}\frac{\partial}{\partial r}\left(r\mu_e \frac{\partial v}{\partial r}\right) + \frac{\partial}{\partial z}\left(\mu_e \frac{\partial u}{\partial r}\right)$
K	μ_e/σ_K	$G - \rho\varepsilon$
ε	μ_e/σ_ε	$\frac{\varepsilon}{K}(C_1 G - C_2 \rho\varepsilon)$
h	$k/C_p + \mu_t/\sigma_h$	$-S_R$
m	$\rho D + \mu_t/\sigma_m$	0

$$\mu_t = C_D \rho K^2/\varepsilon \quad \text{and} \quad G = \mu_e\left[2\left(\frac{\partial u}{\partial z}\right)^2 + 2\left(\frac{\partial v}{\partial r}\right)^2 + 2\left(\frac{v}{r}\right)^2 + \left(\frac{\partial u}{\partial r} + \frac{\partial v}{\partial z}\right)^2\right].$$

The entrainment velocity v is computed by setting the radial gradient of ρrv equal to zero. The entraining nitrogen is assigned an enthalpy value corresponding to ambient temperature.

At the axis of symmetry, the radial velocity v and the radial gradients of all the remaining flow properties are set to zero.

Across the exit plane, located some 20–25 diameters from the torch exit, the axial pressure gradient is assumed to be zero. Also, the axial gradient of axial and radial velocity is assumed to be zero for each. Since these streamwise gradients are low, any downstream-to-upstream link is negligible. Regarding the other variables, the axial gradients of each are set at zero.

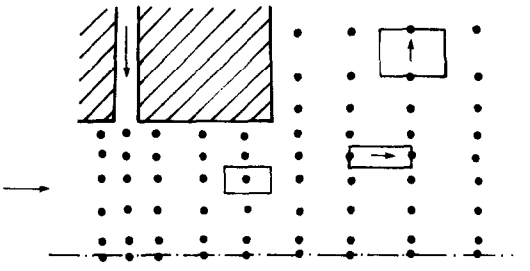

FIG. 2. Layout of the finite difference grid.

SOLUTION PROCEDURE

The solution procedure used is embodied in the basic '2/E/Fix' computer program [18], which provided the starting point from which the present computer program has been developed. The schematic layout of the finite difference grid is shown in Figs. 2 and 3. The velocities are stored at the locations displayed from the main grid points (•) where P, K, ε, m, h. and other auxiliary variables are stored. The partial differential equation for each dependent variable (ϕ) is integrated over the respective control volume (Fig. 3) and the following algebraic equation is obtained for each grid in the calculation domain:

$$A_p\phi_p = A_n\phi_n + A_s\phi_s + A_w\phi_w + A_e\phi_e + S_{\phi.p}. \quad (2)$$

The A's in equation (2) consist of convection and diffusion fluxes through the control volume faces, e.g. A_n contains the convective and diffusive fluxes of ϕ through the north face of the control volume. It was found in the present studies that it was important how these coefficients were calculated for the velocity points adjacent to the nozzle exit corner. Considering the u velocity at point A in Fig. 3, the north coefficient A_n in equation (2) should contain only half the con-

Table 2. Values of turbulence model constants used

C_1	1.43
C_2	1.92
C_D	0.09
σ_K	1.0
σ_ε	1.3
σ_h	0.9
σ_m	0.9

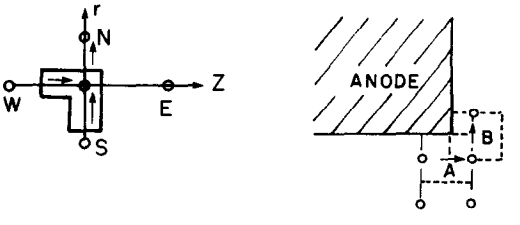

FIG. 3. Detailed layout of the finite difference grid.

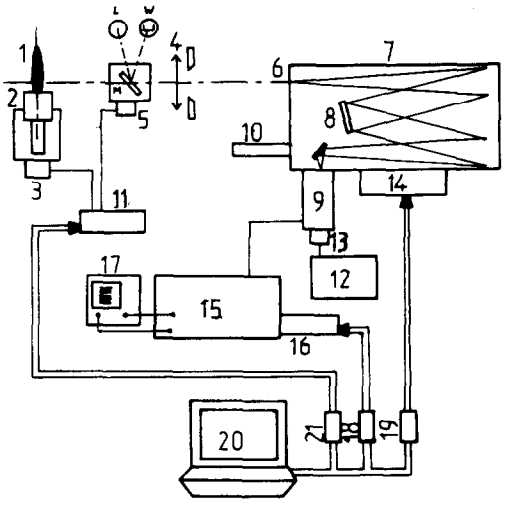

FIG. 4. Experimental arrangement: 1, plume; 2, plasma torch; 3, stepping motor for z motion; 4, lens; 5, stepping motor for M rotation; 6, entrance slit; 7, monochromator; 8, grating; 9, S.I.T. detector; 10, He–Ne laser; 11, clock for stepping motor; 12, H.V. pulse generator; 13, lord; 14, wavelength controller; 15, P.A.R. 1216 controller; 16, interface; 17, scope; 18, 19, 21, interfaces; 20, H.P. 9845 A computer.

vection, since half of the north face of the control volume is blocked by the nozzle surface. Similarly, the diffusion contribution to A_n should be such that it takes account of the fact that half of the north face is the anode wall and only the other half is exposed to the flow. Similar arguments are valid for the west coefficient A_w, considering the v velocity stored at point B.

The computational mesh used for all calculations consisted of 9×11 non-uniformly distributed nodes inside the torch, and 21×30 nodes outside the torch to cover the free plume. The limited grid dependence tests carried out with different arrangements of grid nodes and numbers of grid points showed that any further refinement of the computational grid is unlikely to affect the numerical accuracy of the results presented. A typical run to predict the flow, temperature and concentration field required a cpu time of 1.5 h on a MicroVAX II. The other relevant details of the procedure are described in the earlier paper [1].

The model contains digitized tables for laminar viscosity, density, thermal conductivity, and heat capacity at constant pressure and radiation loss per unit volume of individual gaseous species for the temperature range of interest. The laminar viscosity of the mixture required during computation is estimated using the Wilkes estimate, and the thermal conductivity using Brokaw's method [21]. The heat capacity of the gaseous mixture is obtained using mass fraction weighting. The density of the mixture is obtained using mole-fraction weighting.

EXPERIMENTAL SET-UP

As described in Fig. 4, the plasma jet (1) is imaged using an optical lens (4) with magnification of 1 on the entrance slit (6) of the monochromator (7). We use a Jobin–Yvon THRP monochromator working in first order and single pass with a grating (8) (300, 1800 or 2400 lines mm^{-1}), the angular position of which is monitored by a controller (1) interfaced (19) with the computer (20). For energy and wavelength calibrations, spectral (L) and tungsten ribbon (W) lamps are imaged on the entrance slit using a rotating mirror (M) driven by a stepping motor (5).

The plasma torch (2) is movable along its Z-axis using a stepping motor (M) supplied, as in ref. [5], by an interfaced controller (11). The detection is ensured by a silicon intensified target (9) (S.I.T. Vidicon PAR 1254) driven by a PAR 1216 controller (15) interfaced (16–18) with the computer.

The scanning pattern of the target is viewed on a scope (17) with Wehneit modulation using X–Y–Z outputs of the PAR 1216 controller.

The silicon target of the tube is software divided into different tracks, each of them being assigned to a viewing height from the horizontal jet axis. Moreover, on each track, each channel of the track (up to 511) corresponds to a given wavelength, provided a prior calibration with a spectral lamp and by using the reciprocal dispersion factor of the monochromator. So the O.M.A. with 2-D detector gives both spectral and spatial resolution facilities.

SIGNAL PROCESSING

The thermal background of the silicon target due to electron-hole creation, even with the blind detector, has a highly reproducible level, so that it may be stored in an array of the computer, and then, subtracted from each signal, provided the temperature of the detector and the exposure time are kept constant over the period of the experiment. Arising from the reading mode of the target by an electron beam and from the diffusion of charge carriers in the silicon under illumination, the signal is submitted to crosstalk effects which reduce the resolution of the system. This effect may be accounted for by imaging a very thin light source on a channel location and then scanning the target over the track. This gives rise to an apparatus function which may be included in the further treatment of the data [22]. The spatial resolution is also affected by the light scattered by the collection lens and coming from the brightest part of the jet. As a consequence of the extremely high gradients of brightness, a part of the light emitted by the hottest zone is scattered and overlaps with the light emitted by the fringes of the jet. This gives rise to a flattening of the spatial contour, and this effect is amplified by Abel's inversion. So this scattering effect may be partly accounted for by registering the profile originating from a light source of known dimensions (in our case, a horizontal slit 200 m wide) and standing in the place of the jet. This gives rise, too, to another component of the overall apparatus function by which each signal may be deconvolved using FFT techniques.

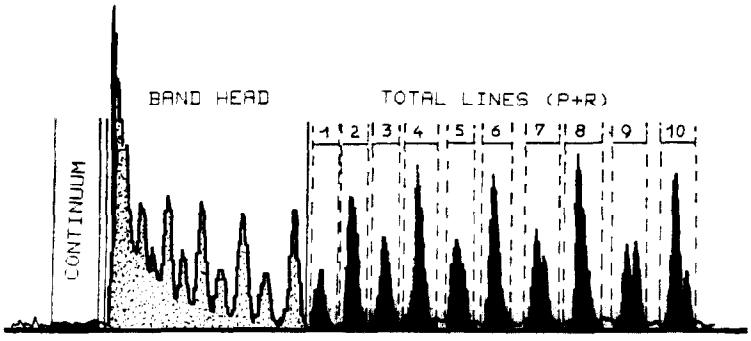

FIG. 5. $N_2^+(1-)$ O–O Band from O.M.R.

Prior to this deconvolution, the signal is noise eliminated by using an optimal Wiener filter as described in ref. [23].

TEMPERATURE MEASUREMENTS

We have measured the rotational temperature which is close to the temperature of heavy species (relaxation time between rotation and translation being less than 10^{-8} s) and which is mainly responsible for heat transfer between the plasma and a solid.

For the temperature measurements, we use the (O–O) transition of the molecular spectra of N_2^+, that is the first negative system.

This requires a good knowledge of the band structure and a fine location of the lines on the target. After wavelength calibration, each line is assigned to stay, on each track, in a given domain defined by its mean location and its width, both expressed in channel number. According to the resolution we use (about 0.2 A), the molecular spectrum consists of an unresolved hand head including the first 26 P lines, and partially resolved total lines, each of these including P and R overlapping lines. Such a spectrum is presented in Fig. 5, as plotted by the computer after data acquisition.

Neglecting the spin doubling, we may write the emission coefficient for P and R lines as [24]

$$\varepsilon_P(T) = C\phi\sigma^4 K_P \exp\left(-\frac{hc}{kT}F'(K_P-1)\right) \quad (3)$$

$$\varepsilon_R(T) = C\phi\sigma^4(K_R+1)\exp\left(-\frac{hc}{kT}F'(K_R+1)\right) \quad (4)$$

with

$$C = \frac{16}{3}\pi^3 c\frac{N(T)}{Q(T)}S_{n'v'}^{n''v''}\exp\left(-\frac{hc}{kT}(T_e'+G'(v'))\right) \quad (5)$$

where $\phi = 2/3$ for odd values of K, 1/3 in the other case; K the rotational quantum number of the lower level; σ the wave number of the line; $S_{n'v'}^{n''v''}$ the band strength; and T_e', $G'(v')$ and $F'(K)$ are the electronic, vibrational and rotational spectral terms, respectively, of the upper level.

In Fig. 5, the lines indexed 1–10 are the result of the overlapping of a P line and an R line such as $K_P = K_R + 27$, and starting from $K_R = 0$.

The method we use for the rotational temperature measurement is briefly summarized as follows. The only assumption we need is that the rotational relaxation is fast enough to allow a Boltzmann distribution among the rotational levels.

Summing the spectral emission coefficient over the range corresponding to the band head, we get

$$\varepsilon_{head} = \sum_{K_P=1}^{26}\varepsilon_P(T). \quad (6)$$

Then, summing the spectral emission coefficient over the domain allocated to each (P+R) line, indexed i, we get

$$\varepsilon_{line\text{-}i} = \varepsilon_{P_i}(T) + \varepsilon_{R_i}(T). \quad (7)$$

Thus, for each line we define as a theoretical function of the temperature, the relative coefficient

$$I_i^{th}(T) = \frac{\varepsilon_{line\text{-}i}(T)}{\varepsilon_{head}(T)} \quad (8)$$

which is independent of $N(T)$, $Q(T)$ and $S_{n'v'}^{n''v''}$.

After the registration and the brightness calibration of the spectrum, Abel's inversion for the band head, the line and the continuum, we get a set of experimental values for each relative emission coefficient, and this for each track. It can be expressed by

$$I_i^{exp}(T) = \frac{\varepsilon_{line\text{-}i}^{exp}}{\varepsilon_{head}^{exp}}. \quad (9)$$

The temperature is then calculated as the parameter which minimizes the quantity

$$E(T) = \frac{1}{N}\left[\sum_{i=1}^{N}(I_i^{exp}-I_i^{th}(T))^2\right]^{1/2} \quad (10)$$

N being the number of the (P+R) lines under analysis.

The precision of the measurements is evaluated by using the curvature of the $E(T)$ function in its minimum neighborhood and the value of this minimum.

More specifically, the temperature is determined from the rotational spectrum of the N_2^+ (O–O) band and by an adjustment of the experimental measurements with a set of theoretical spectra computed for

different temperatures. The squared deviation is then given as a function of the temperature from which the theoretical spectrum is computed. This function, $E_q(T)$, shows a minimum for the best guess, T_m, and this minimum would be zero if the measurements were perfect. In reality, this is never the case and the minimum of $E_q(T)$ is a non-zero value, E_m. From this value, and from the curvature of the function in the neighborhood of T_m, we can evaluate the quantity

$$\delta T = \sqrt{\left(\frac{2E_m}{(\partial^2 E_q/\partial T^2)}\right)} \tag{11}$$

which reflects the quality of the measurement rather than a real error. The value of E_m is related to the S/N ratio and $(\partial^2 E_q/\partial T^2)$ to the sensitivity of the method.

As the relative evolution of the intensities of the lines in the band is more sensitive to the temperature variations at low temperatures, the sensitivity is improved in the cold regions of the jet. In contrast, when the temperature decreases (typically below 5000 K), the line intensity decreases and, at the same time, the noise, mainly due to the plasma fluctuations in the fringes, increases; E_m increases too.

In order to show how the accuracy of the measurements changes from point to point, the idea was to plot the experimental isotherms as bands. It should be noted that the width of each band depends on both the intrinsic accuracy and on the temperature gradient.

Let ρ be the radius of curvature at each point of a given isotherm T. Along the radius the variation δT of T is reflected by a quantity $\delta\rho$ which may be evaluated as follows:

$$\delta T = \left(\frac{\partial T}{\partial n}\right)\delta\rho \tag{12}$$

where $(\partial T/\partial n)$ is the normal derivative of the temperature.

For example, on the jet axis in the range 6.7 kK, the recombination of atomic nitrogen plays the role of a thermal buffer, and thus the temperature gradient is low in this region. As a consequence for a given value of δT, the width $\delta\rho$ will be large even though the accuracy is good. In the 6–7 kK region close to the nozzle exit, the accuracy of the measurements is about the same, but in this case the gradient is very steep. Consequently, the $\delta\rho$ width is lower than the previous case. Finally, in the 3–4 kK region for large Z values, the sensitivity is very good (low temperature) but the signal is weak, instabilities are large and radial gradient steep; $\delta\rho$ is increasing with Z.

A COMPARISON OF MEASUREMENTS AND PREDICTIONS

In this section, we shall consider a critical comparison of the theoretical predictions with experimental measurements. We shall be considering three sets of measurements, namely:

(1) a nitrogen jet discharging into nitrogen (depicted in Figs. 6–8);

(2) a nitrogen jet discharging into nitrogen with a sideways injection of a nitrogen stream (depicted in Figs. 9–11);

(3) a nitrogen jet discharging into nitrogen with a sideways injection of an oxygen stream (depicted in Figs. 12–14).

These measurements, including the facts that the power input and the gas flow rates were made to vary within each individual set, represent a broad enough range of conditions to provide realistic perspectives regarding the assessment of the modelling effort.

Figures 6–8 represent conditions corresponding to the behavior of a 'straight' plasma jet; problems of this type have been tackled both by previous investigators and the present authors. Here, Figs. 6 and 8 represent essentially identical conditions, shown here in order to indicate the reproducibility of the experimental measurements. The situation depicted in Fig. 7 corresponds to a nearly 50% increase in the gas flow rate, and an increase of about 20% in the power input.

Inspection of these plots shows fairly good agreement regarding the general trends exhibited; the agreement regarding the jet boundaries, as signified by the 3 kK isotherm, is excellent.

The principal discrepancies between the measurements and the predictions lie in the entrance region; to a significant extent, this may be attributable to the difficulties involved in specifying realistic inlet boundary conditions. As discussed in the preceding section, in the calculations the domain of integration included some inside portion of the torch; however, the problems will not be completely resolved until the whole torch is included in the calculations. Another potential source of the discrepancy is the inherent difficulty in making precise temperature measurements in a region where extremely steep temperature gradients exist. In this regard, the 3 or 4 kK boundary is much easier to resolve. Further reasons for the discrepancy may include asymmetric torch behavior and possibly the departure from local thermodynamic equilibrium.

Figures 9–11 show a system with a sideways injection of nitrogen. As seen in the captions, the volumetric flow rate of the injected stream is significantly less than that of the main plasma jet. This arrangement will lead to a rather more complicated flow pattern, and one would expect on physical grounds that the outer regions of the plasma jet would be cooled by the injected stream. Both the experimental and the computed results reflect this trend.

Finally, Figs. 12–14 depict systems where an oxygen stream is being injected. Oxygen will be a more effective coolant in this instance because of its higher specific heat closely connected to its higher energy of dissociation, at about 4000 K against 7000 K for nitrogen, resulting in a much higher enthalpy of oxygen at 4000 K than of nitrogen at the same temperature. Indeed, inspection of these figures shows that

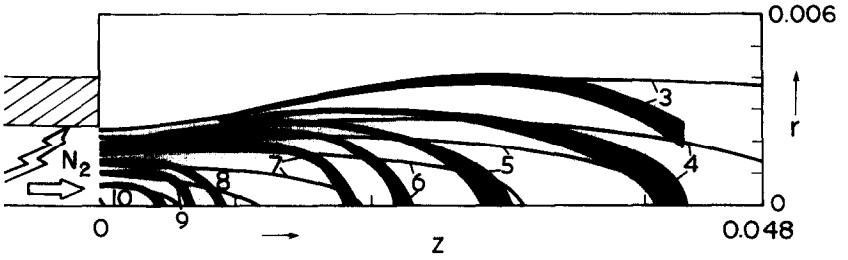

FIG. 6. Comparison of experimentally measured and theoretically predicted temperature profiles for a nitrogen plasma jet discharging into nitrogen. Measurements are given by the broad curves (Q_p = 20 l m^{-1}; P_w = 11.6 kW; η = 59%).

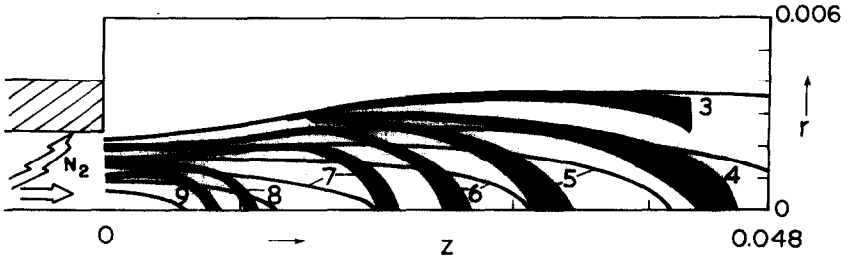

FIG. 7. Comparison of experimentally measured and theoretically predicted temperature profiles for a nitrogen plasma jet discharging into nitrogen. Measurements are given by the broad curves (Q_p = 30.4 l m^{-1}; P_w = 13.4 kW; η = 59%).

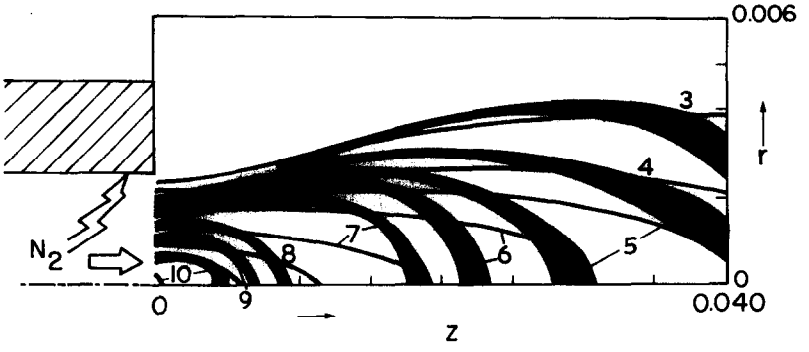

FIG. 8. Comparison of experimentally measured and theoretically predicted temperature profiles for a nitrogen plasma jet discharging into nitrogen. Measurements are given by the broad curves (Q_p = 20 l m^{-1}; P_w = 11.4 kW; η = 59%).

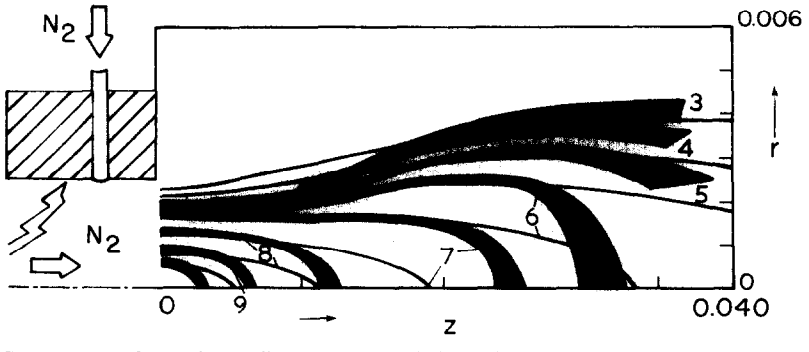

FIG. 9. Comparison of experimentally measured and theoretically predicted temperature profiles for a nitrogen plasma jet discharging into nitrogen, with a sideways injection of a cold nitrogen stream. Measurements are given by the broad curve (Q_p = 20 l m^{-1}; P_w = 11.6 kW; Q_i = 2 l m^{-1}; η = 59%).

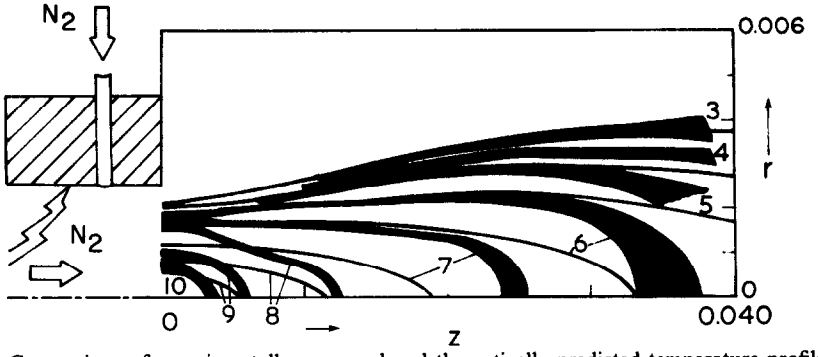

FIG. 10. Comparison of experimentally measured and theoretically predicted temperature profiles for a nitrogen plasma jet discharging into nitrogen, with a sideways injection of a cold nitrogen stream. Measurements are given by the broad curve ($Q_p = 20\,l\,m^{-1}$; $P_w = 11.6$ kW; $Q_i = 4\,l\,m^{-1}$; $\eta = 59\%$).

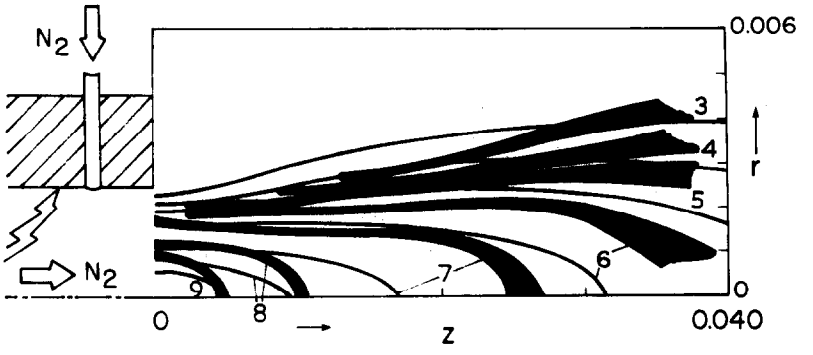

FIG. 11. Comparison of experimentally measured and theoretically predicted temperature profiles for a nitrogen plasma jet discharging into nitrogen, with a sideways injection of a cold nitrogen stream. Measurements are given by the broad curve ($Q_p = 10.6\,l\,m^{-1}$; $P_w = 9.8$ kW; $Q_i = 4\,l\,m^{-1}$; $\eta = 45\%$).

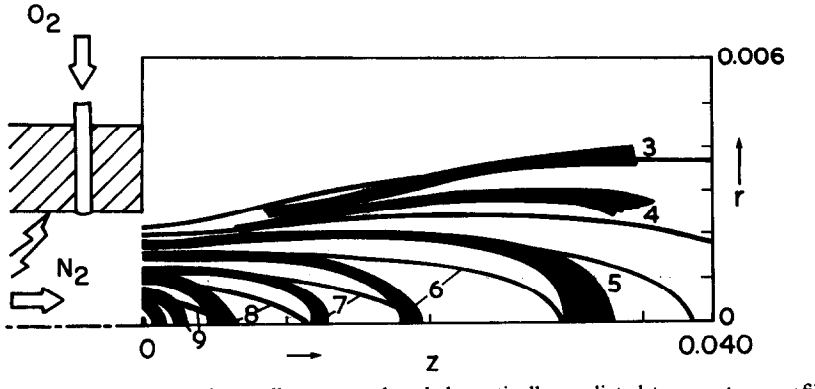

FIG. 12. Comparison of experimentally measured and theoretically predicted temperature profiles for a nitrogen plasma jet discharging into nitrogen, with a sideways injection of a cold oxygen stream. Measurements are given by the broad curve ($Q_p = 20\,l\,m^{-1}$; $P_w = 11.6$ kW; $Q_i = 2\,l\,m^{-1}$; $\eta = 59\%$).

the jet boundaries are being 'squeezed inwards', especially at the higher oxygen input rates. The experimental measurements and the theoretical predictions are in good agreement regarding this trend.

Computed axial velocity profiles are presented as Figs. 15 and 16 for identical plasma gas flow rate and torch power but for cold oxygen flow rate Q_i, equal to 2 and 7 $l\,m^{-1}$, respectively. The marked influence of cold gas injection on velocity field is readily apparent. Figures 17 and 18 depict the computed oxygen fields for these two values of flow rates for sideways-injected oxygen. The oxygen fields presented are consistent with the expected behavior. The purpose of showing these profiles is to demonstrate the ability of the program to represent flow field and mixing also, which information is needed for the understanding of virtually all practical plasma systems.

DISCUSSION

In this paper a critical comparison is presented of theoretical predictions and experimental measure-

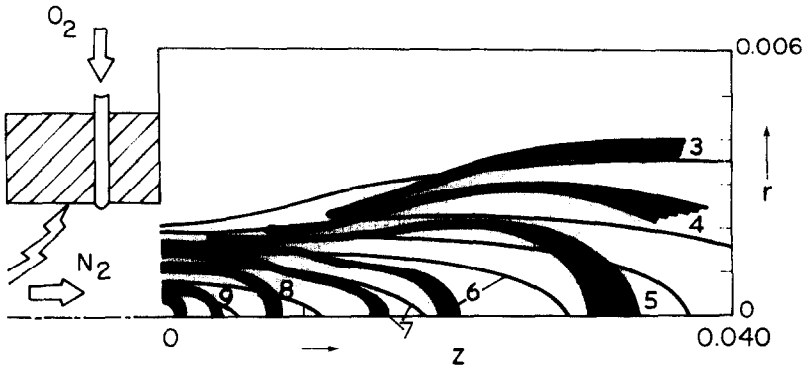

FIG. 13. Comparison of experimentally measured and theoretically predicted temperature profiles for a nitrogen plasma jet discharging into nitrogen, with a sideways injection of a cold oxygen stream. Measurements are given by the broad curve ($Q_p = 20\,l\,m^{-1}$; $P_w = 11.6$ kW; $Q_i = 4\,l\,m^{-1}$; $\eta = 59\%$).

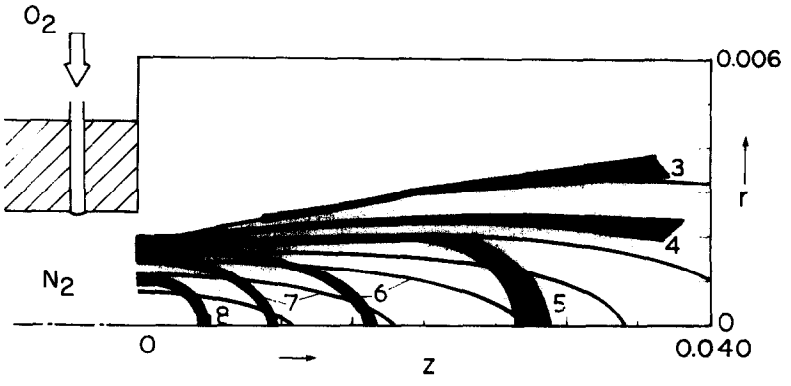

FIG. 14. Comparison of experimentally measured and theoretically predicted temperature profiles for a nitrogen plasma jet discharging into nitrogen, with a sideways injection of a cold oxygen stream. Measurements are given by the broad curve ($Q_p = 20\,l\,m^{-1}$; $P_w = 11.6$ kW; $Q_i = 7\,l\,m^{-1}$; $\eta = 59\%$).

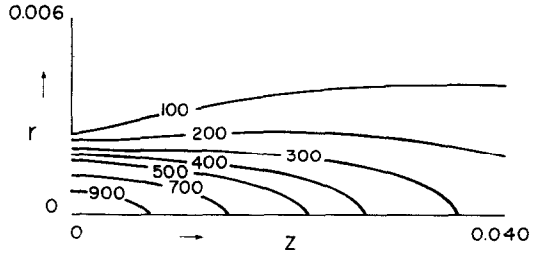

FIG. 15. Computed axial velocity field for a nitrogen plasma jet discharging into nitrogen, with a sideways injection of a cold oxygen stream ($Q_p = 20\,l\,m^{-1}$; $P_w = 11.6$ kW; $Q_i = 2\,l\,m^{-1}$; $\eta = 59\%$).

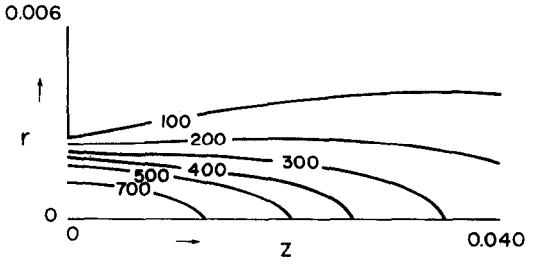

FIG. 16. Computed axial velocity field for a nitrogen plasma jet discharging into nitrogen, with a sideways injection of a cold oxygen stream ($Q_p = 20\,l\,m^{-1}$; $P_w = 11.6$ kW; $Q_i = 7\,l\,m^{-1}$; $\eta = 59\%$).

ments concerning the temperature profiles in a nitrogen plasma jet discharging into nitrogen, with a sideways injected cold gas stream.

In general, the theoretical predictions were found to be in quite good agreement with the measurements; indeed, this agreement has been rather better than found by previous investigators. Reasons for this are thought to include the following.

(1) In the formulation of the problem, particular care has been taken in the definition of the temperature and the velocity profiles at the inlet to the domain of the integration; this was found to be quite critical.

(2) In the solution of the problem, care has been taken to satisfy the overall heat and mass balances; this issue may appear trivial, but it has not received as much attention as necessary in the past.

(3) In the development of the numerical scheme, care has been taken to provide a proper representation of the boundaries, especially in the corner regions near the inlet, i.e. the nozzle exit.

Even allowing for the obvious difficulties inherent in making accurate temperature measurements, significant discrepancies still remain between measurements and predictions, especially in the regions adjac-

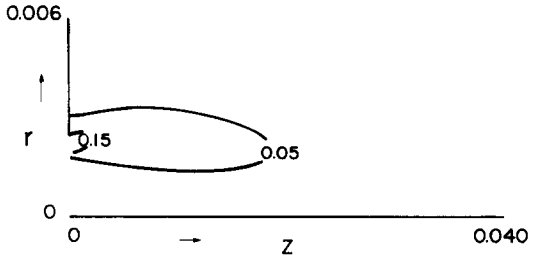

FIG. 17. Computed oxygen field for a nitrogen plasma jet, with a sideways injection of a cold oxygen stream (Q_p = 20 l m^{-1}; P_w = 11.6 kW; Q_i = 2 l m^{-1}; η = 59%).

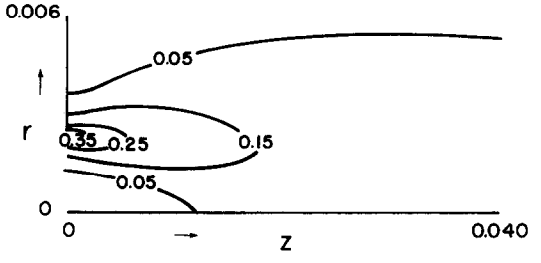

FIG. 18. Computed oxygen field for a nitrogen plasma jet, with a sideways injection of a cold oxygen stream (Q_p = 20 l m^{-1}; P_w = 11.6 kW; Q_i = 7 l m^{-1}; η = 59%).

ent to the plasma jet nozzle. These problems are inherently associated with the need to have a precise knowledge of the velocity and the temperature fields within the plasma gun and will not be resolvable until this issue is specifically addressed. The second, only partially resolved problem is associated with the laminar–turbulent transition within the chamber. For the conditions considered, the plasma jet is laminar in the nozzle, but will become turbulent some distance downstream from the nozzle exit.

Resolution of these problems poses a major challenge, but work is proceeding in both these areas.

Acknowledgements—The authors wish to thank the U.S. Department of Energy for partial support of this investigation under Grant No. DE-FG02-85ER-13331, and the United States Education Foundation in Pakistan and Council for International Exchange of Scholars in Washington, DC.

REFERENCES

1. A. H. Dilawari and J. Szekely, Fluid flow and heat transfer in plasma reactors—I. Calculation of velocities, temperature profiles and mixing, *Int. J. Heat Mass Transfer* **30**, 2357–2372 (1987).
2. Y. C. Lee, Modelling work in thermal plasma processing, Ph.D. Thesis, University of Minnesota (1984).
3. C. P. Donaldson and K. E. Gray, Theoretical and experimental investigation of the compressible free mixing of two dissimilar gases, *AIAA J.* **4**, 2017–2025 (1966).
4. M. I. Boulos and W. H. Gauvin, Powder processing in a plasma jet: a proposed model, *Can. J. Chem. Engng* **52**, 355–363 (1974).
5. S. M. Correa, Transitional plasma jet modelling, ISPC-6, Montreal, Vol. 1, pp. 77–82 (1983).
6. J. McKelliget, J. Szekely, M. Vardelle and P. Fauchais, Temperature and velocity fields in a gas stream exiting a plasma torch: a mathematical model and its experimental verification, *Plasma Chem. Plasma Processing* **2**, 317–332 (1982).
7. A. H. Dilawari and J. Szekely, Some perspectives on the modelling of plasma jets, *Plasma Chem. Plasma Processing* 7(3), 317–339 (1987).
8. B. E. Launder and D. B. Spalding, The numerical computation of turbulent flows, *Comput. Meth. Appl. Mech. Engng* **3**, 269–289 (1974).
9. K. Y. Chien, Predictions of channel and boundary-layer flows with a low-Reynolds number turbulence model, *AIAA J.* **20**, 33–38 (1982).
10. S. Hassid and M. Porch, A turbulent energy dissipation model for flows with drag reduction, *J. Fluids Engng* **100**, 107–112 (1978).
11. G. H. Hoffman, Improved form of the low-Reynolds number K–ε turbulence model, *Physics Fluids* **18**, 309–312 (1975).
12. C. K. G. Lam and K. A. Bremhorst, Modified form of the K–ε model for predicting wall turbulence, *J. Fluids Engng* **103**, 456–460 (1981).
13. W. P. Jones and B. E. Launder, The prediction of laminarization with a two-equation model of turbulence, *Int. J. Heat Mass Transfer* **15**, 301–314 (1972).
14. B. E. Launder, A. Morse, W. Rodi and D. B. Spalding, The prediction of free shear flows: a comparison of the performance of six turbulent models, NASA SP-321 (1972).
15. A. J. Favre, Equations des gaz turbulents compressibles, *J. Méc.* **4**, 361 (1965).
16. P. Fauchais, Private communication (1986).
17. J. M. Yos, Technical Memorandum RAD-TM-63-7, Research and Advanced Development, AVCO Corporation, Wilmington, Massachusetts (1963).
18. W. M. Pun and D. B. Spalding, A general computer program for two-dimensional elliptic flows, Rep. No. HTS/76/2, Heat Transfer Section, Imperial College, London (1976).
19. M. A. Leschziner and W. Rodi, Calculation of annular and twin parallel jets using various discretization schemes and turbulence-model variations, *Trans. ASME: J. Fluid Engng* **103**, 352–360 (1981).
20. M. A. Leschziner and W. Rodi, Computation of strongly swirling axisymmetric free jets, *AIAA J.* **22**(12), 1742–1747 (1984).
21. R. C. Reid, J. M. Prausnitz and T. K. Sherwood, *The Properties of Gases and Liquids*. McGraw-Hill, New York (1977).
22. P. Meyer and J. Bures, Comportement thermique d'une ligne de microphotodiodes, *Appl. Opt.* **19**, 86–91 (1980).
23. E. L. Kosarev and E. Pantos, Optimal smoothing of 'noisy' data by fast Fourier transform, *J. Phys. E. Scient. Instrum.* **16**, 537–543 (1983).
24. G. Herzberg, *Spectra of Diatomic Molecules*. Van Nostrand, New York (1950).

ECOULEMENT ET TRANSFERT DE CHALEUR DANS DES REACTEURS A PLASMA—II. COMPARAISON CRITIQUE DES PROFILS DE TEMPERATURE CALCULES ET EXPERIMENTAUX DANS DES JETS DE PLASMA EN L'ABSENCE OU EN PRESENCE D'INJECTION LATERALE

Résumé—On présente une comparaison critique entre des mesures expérimentales et des calculs de profils de température dans un jet de plasma d'azote débouchant dans de l'azote, avec un écoulement froid latéral d'azote ou d'oxygène gazeux. En général, les prévisions basées sur la résolution des équations axi-symétriques de Navier–Stokes associées aux équations de bilan de masse et d'énergie, sont trouvées être en bon accord avec les mesures. Comme originalité du modèle est l'attention particulière portée à la spécification des profils de température et de vitesse à l'entrée, à une certaine distance à l'intérieur de la torche, et des conditions aux limites thermiques sur les autres frontières.

STRÖMUNG UND WÄRMEÜBERGANG IN PLASMA-REAKTOREN—II. KRITISCHER VERGLEICH ZWISCHEN GEMESSENEN UND BERECHNETEN TEMPERATURPROFILEN IN PLASMASTRÖMEN

Zusammenfassung—Es wird ein kritischer Vergleich zwischen experimentellen Ergebnissen und theoretischen Berechnungen vorgestellt für den Temperaturverlauf in einem Stickstoffplasma-Strahl. Der Plasmastrahl tritt in Stickstoff ein, wobei ihm seitlich kaltes Stickstoff- oder Sauerstoff-Gas zugeführt wird. Die Lösung der achsensymmetrischen Navier–Stokes-Gleichungen und der zugehörigen Energie- und Massenbilanzbeziehungen stimmen gut mit den Messungen überein. Das Besondere an dieser Arbeit ist, daß die Temperatur- und Geschwindigkeitsprofile am Eintritt und die thermischen Randbedingungen an den anderen Berandungen besonders sorgfältig gewählt werden.

ТЕЧЕНИЕ ЖИДКОСТИ И ТЕПЛОПЕРЕНОС В ПЛАЗМЕННЫХ РЕАКТОРАХ-II. КРИТИЧЕСКОЕ СОПОСТАВЛЕНИЕ ЭКСПЕРИМЕНТАЛЬНО ИЗМЕРЕННЫХ И ТЕОРЕТИЧЕСКИ РАССЧИТАННЫХ ПРОФИЛЕЙ ТЕМПЕРАТУРЫ В ПЛАЗМЕННЫХ СТРУЯХ В ОТСУТСТВИЕ И ПРИ НАЛИЧИИ ВДУВА СБОКУ

Аннотация—Представлено критическое сопоставление экспериментальных данных и теоретических расчетов, описывающих профили температуры в плазменной струе азота, истекаемой в азот, при боковом вдуве потока холодного азота или кислорода. В целом найдено, что теоретические расчеты на основе решения осесимметричных уравнений Навье–Стокса и выражений для теплового и массового баланса хорошо согласуются с данными измерений. Особенностью моделирования описываемого процесса является то, что большое внимание уделялось точному определению профилей температуры и скорости на границе вдува, взятой на некотором расстоянии внутри горелки, а также определению тепловых граничных условий на других ограничивающих поверхностях.